

Validation of a light field camera for investigation on complex plasma

SONJA MAIER¹

¹Deutsches Zentrum für Luft- und Raumfahrt e.V. (DLR), Institut für Materialphysik im Weltraum, Gruppe Komplexe Plasmen, 2017, 82234 Wessling, Germany

Abstract: Ekoplasma is going to be the fourth-generation laboratory for the investigation of complex plasmas under microgravity conditions on the International Space Station (ISS). For the first time, particle motion is aimed to be observed three-dimensional by a light field camera under microgravity. The main features of a light field camera were explored. And a three-dimensional calibration target for the validation process was designed and approved. Overall, due to its design this target provides the same capabilities for every imaging system. It therefore is a universal device that will help to develop and classify an imaging system applicable for three dimensional plasma research on the ISS.

© 2017 Optical Society of America

References and links

1. Knapek C. A. , Huber P. , Mohr D. P. , Zaehring E. et al., "Ekoplasma - Experiments with Grid Electrodes in Microgravity," AIP Conference Proceedings, 8th International Conference on the Physics of Dusty Plasmas (2017).
 2. Nefedov A. P., Morfill G. E., Fortov V. E., Thomas H. M. et al., "PKE-Nefedov: plasma crystal experiments on the International Space Station," New Journal of Physics 5 (2003).
 3. Sun J., Xu C., Zhang B., Hossain M., Wang S., Qi H., and Tan H., "Three-dimensional temperature field measurement of flame using a single light field camera," Opt. Express 24, 1118-1132 (2016).
 4. Ding Y., Yu J., Sturm P., "Multiperspective Stereo Matching and Volumetric Reconstruction," IEEE 12th International Conference on Computer Vision (2009).
 5. Gortler, S. J., Grzeszczuk, R., Zeliski, R., Cohen, M. F., "The lumigraph," Proceedings of the 23rd annual conference on computer graphics and interactive techniques, 43-54 (1996).
 6. Georgiev T., Lumsdaine A., "The multifocus plenoptic camera," Proc.SPIE 8299, 8299 - 8299 - 11 (2012).
-

1. Introduction

Imaging systems play a major role in fundamental research, since they are used for data acquirement and analysis. In the framework of the Ekoplasma project (see [1]) on the Institute of Material Physics in Space at the German Aerospace Center (DLR), the Complex Plasma group resorts to imaging systems in order to investigate particle motion and phase transitions in complex plasmas. A complex plasma is an ionized gas that contains highly charged microparticles. In microgravity, the microparticles spread unhindered in space and form consecutive three-dimensional structures. The particles behave likewise to atoms in a gaseous liquid or solid state – with the advantage that each microparticle in the plasma can be observed separately. This provides an entire new insight into fundamental physics (see [2]). Hence the imaging system has to manage the challenge to observe and track single microparticles in three dimensions. Therefore, Ekoplasma research group invested in the lately enhanced light field camera technology to attain best data sourcing at minimal space requirements. A R5 light field camera was purchased from manufacturer Raytrix¹, who also provides software for different analyze purposes. However, it is not clear whether the present light field (LF) camera is favorable to do particle tracking in complex plasmas. Until now it is not possible to extract useful information from data which was taken during a parabolic flight. Hence, the aim of this internship is to design a validation procedure that allows to investigate the properties of the present imaging system and infer whether the R5 light field camera is suitable to study particle motion and phase transitions in complex plasmas.

¹Raytrix GmbH, www.raytrix.de up-to-date: July, 2017, founded in 2008, Kiel, Germany.

2. Theory

2.1. Principles of light field cameras

When a multi lens array (MLA) is embedded inside a regular camera the camera gains a multi perspective stereo view and the ability to capture the light field density of a volume instead of the two-dimensional top view. Because every thin bundle of rays is captured separately. Therefore, the intensity is a function of sensor position and represents the light field density as a function of the direction of incidence (see [3]).

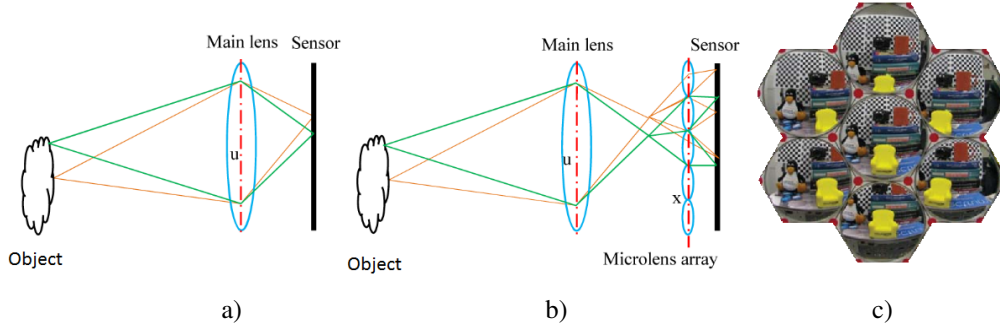


Fig. 1: Figure a) shows a traditional camera that captures an image by collecting the intensities of all rays striking on each sensor pixel. Figure b) shows a schematic of a LF camera where the intensity is a function of sensor position and represents the light field density as a function of the direction of incidence (see [3]). Figure c) points out that the scene captured by each lens is captured from a slightly different angle of vision with computation that leads to a three-dimensional image (see [4]).

Figure 1 shows the principle of beam propagation in a LF camera in contrast to the beam propagation in a traditional camera. In general, the static and non time dependent light field density reflected by an object can be described with a plenoptic function that depends on three spacial (x, y, z) and two angular parameters (θ, ϕ) . A valid approximation is that light rays maintain a constant light density along the direction of propagation (z) hence this direction can be neglected and a four dimensional plenoptic function is sufficient to describe the radiance $r(q, p)$ as a function of position $q(x, y)$ and direction $p(\theta, \phi)$. [5] The radiance $r(q, p)$ of discrete bundles of rays at the image plane is sampled on distinct pixels. Given the radiance $r(q, p)$, a three-dimensional image $I(q)$ can be rendered for a given range of available directions p according to Equation 1.

$$I(q) = \int r(q, p) dp \quad (1)$$

2.2. The R5 light field camera

The main peculiarity of the R5 is the multi focus MLA, that is to improve the depth of field of the camera. In particular, the MLA of the R5 consists from three different sets of microlenses each of them with a characteristic focal length. The three sets are interlaced on an array. The advantage is evident; the recorded scene can be recovered from three different focal planes. The focal planes itself have a distinct relation, therefore computation allows refocusing of the image after a picture was taken. When the collected data from all focal planes are used, a scene can be synthesized in total focus. This enhancement is traded off against lateral resolution because instead of one focal plane three focal planes collect data on the same CMOS (complementary metal-oxide-semiconductor) chip. As they share the area of the CMOS chip they have at most one third of the resolution of the CMOS chip. The lateral resolution is further restricted to the area where the rectangular pixels of the CMOS chip are covered with circular microlenses. The regions between lenses can not be used for data acquisition, this degradation as well as the principle of

multi focus is visualized in Figure 2. The actual arrangement of the microlenses on the array depends on camera construction, maximal filling factor of the pixels as well as the different focal lengths; the lens arrangement of the R5 MLA is realized in a honey comb structure and patented. Manufacturer raytrix denied to give more information on the individual focal lengths (see [6]).

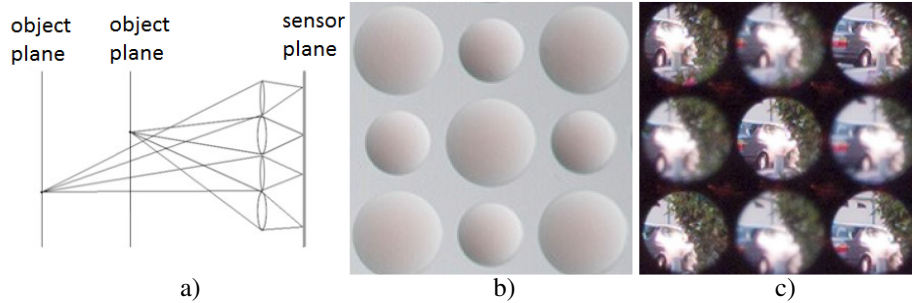


Fig. 2: Figure a) illustrates the ray paths from two object planes onto the same CMOS sensor. Figure b) show a MLA with two focus lengths. c) shows the corresponding images captured on a sensor, the image plane in focus clearly changes. The black regions between the lenses can not be used to collect data on the CMOS chip (see [6]).

3. Preliminary investigations

For optimal usage of the imaging system it is of interest with what precision it can collect data. Hence some preliminary tests regarding the field of view, depth resolution and working distance are carried out. Due to different main topic and limited internship period they are not complete.

- **Working distance of the R5:** Since the multifocus MLA is embedded in an optical system that contains an unknown upstream collector lens. The focal planes can not be measured directly. Besides, the working distances are more relevant to make use of the LF system. The three working distances are measured with a number on a back illuminated 1951 USAF resolution target that is placed parallel to the cameras image sensor and (119 ± 0.2) mm in front of the camera. For one set of microlenses this distance delivers a focused image on the sensor. The distance between the target and the camera is moved until the image of the raw picture in the two remaining lens sets is sharp. The three planes are (2 ± 0.01) mm and (6 ± 0.01) mm apart from the first plane. The raw images as well as the reconstructed images in total focus can be seen in Figure 3. Best image in total focus in terms of sharpness is achieved in a distance of (123 ± 0.2) mm in front of the camera.

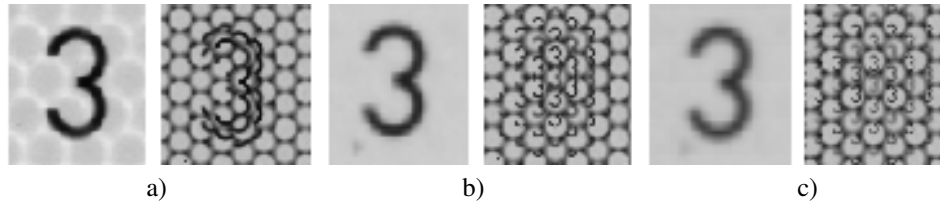


Fig. 3: Left picture of each pair is the reconstructed image in total focus. Pictures on the right hand side of the pairs represent the raw image captured by the sensor; while c) corresponds to the closest and a) to the most far working distance.

- **Lateral field of view:** The lateral field of view is defined as the range for that the camera is sensitive to incident radiation. It is determined only in the focal plane with a specific line from the 1951 USAF resolution target that is moved in x and y direction. The bandwidth

for that the edge line can be reconstructed in each direction is interpreted as the field of view of the LF camera. The field of view is found to be (14.0 ± 0.1) mm in x-direction and (14.0 ± 0.1) mm in y-direction. The directional nomenclature is consistent with Figure 10.

- **Lateral Resolution:** Overall lateral resolution in total focus is measured with a back illuminated 1951 USAF resolution target that is placed parallel in front of the image sensor. Figure 4 shows the mean value of the brightness control of several horizontal and vertical line pair (lp) patterns of USAF group 4. The brightness control of element 4 features the curve progression of three dark and two bright bars while element 5 shows a different curve progression. For element 5 the bars can not be recovered from the brightness control.

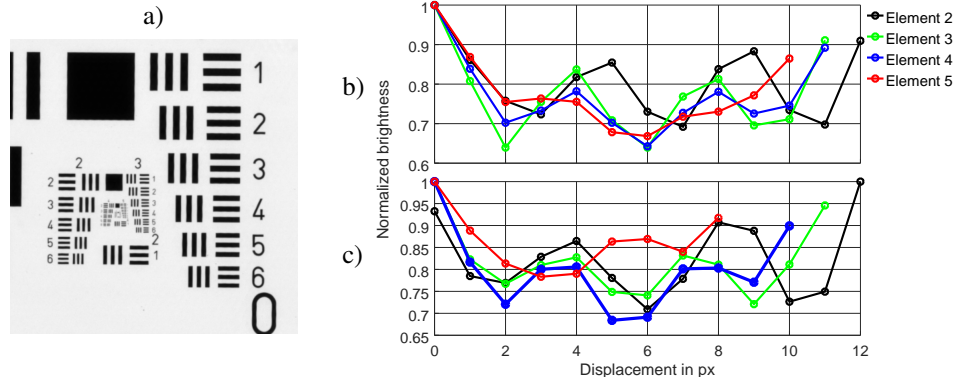


Fig. 4: Figure a) shows an image section of the 1951 USAF resolution target in total focus. b) gives the brightness control of vertical line pairs and c) the brightness control for horizontal line pairs in USAF group 4.

- **Depth resolution:** Depth of field (DOF) resolution can be measured with a gauged depth of field target² that is placed in front of the camera. The target is viewed at 45° . Figure 5 a) shows the picture of the DOF target in total focus taken with the R5.

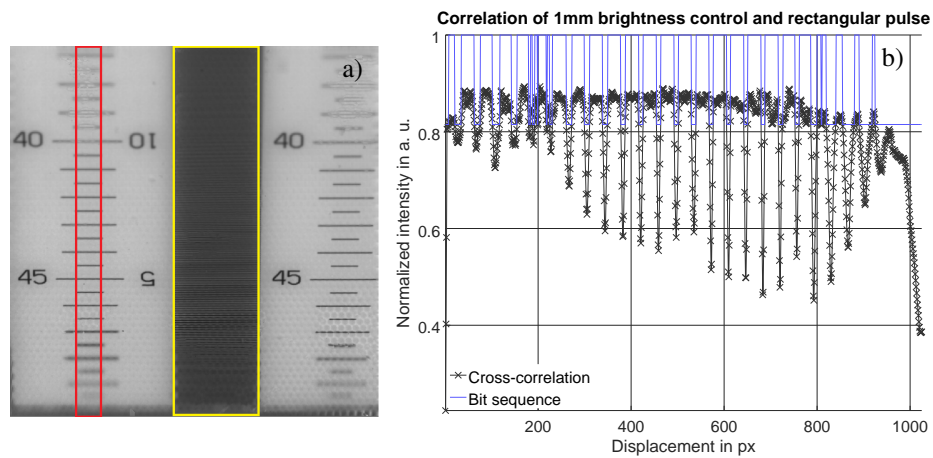


Fig. 5: Figure a) shows an image section of the DOF target in total focus. Red rectangle marks the 1 mm scale and yellow rectangle marks the most delicate pattern with $15 \frac{lp}{mm}$. Figure b) gives the cross-correlation of brightness control of the 1 mm pattern with a rectangular pulse. Bit sequence illustrates visible peaks, for that the cross-correlation exceeds a threshold.

²Depth of Field Target 5-15 manufactured by Edmund Optics. Item number: 54-440

Brightness control over the red framed 1 mm scale is measured. Pattern matching with a tight rectangular pulse using cross-correlation is evaluated. A threshold is derived from the signal and compared to the cross-section. Values that exceed the threshold are one, other values are zero. This results in a bit sequence. Figure 5 b) shows the bit sequence shifted by one and multiplied with the threshold; 14 peaks with about the same width are clearly visible. Consequential, the depth of field is about 14 mm for patterns with an accuracy of 1 mm in the center of the collected image. Beyond that, the target has three fixed line pair patterns. To gain the best insight about the depth resolution the brightness control of the most delicate pattern with $15 \frac{\text{lp}}{\text{mm}}$ framed in yellow (see Figure 5) is recorded. A signal analysis algorithm using the sliced dot product iterates over the signal and searches and weights the frequencies of continuous cosine functions contained in the signal. The cosine signal with the most present high frequency of $210 \frac{1}{\text{px}}$ corresponds to the $15 \frac{\text{lp}}{\text{mm}}$ pattern and is superposed with a detailed sequence in Figure 6. The signals are in phase for about $(234 \pm 15) \text{ px}$ this corresponds to a metric measure of $(3.196 \pm 0.2) \text{ mm}$ and represents the depth of focus for $15 \frac{\text{lp}}{\text{mm}}$.

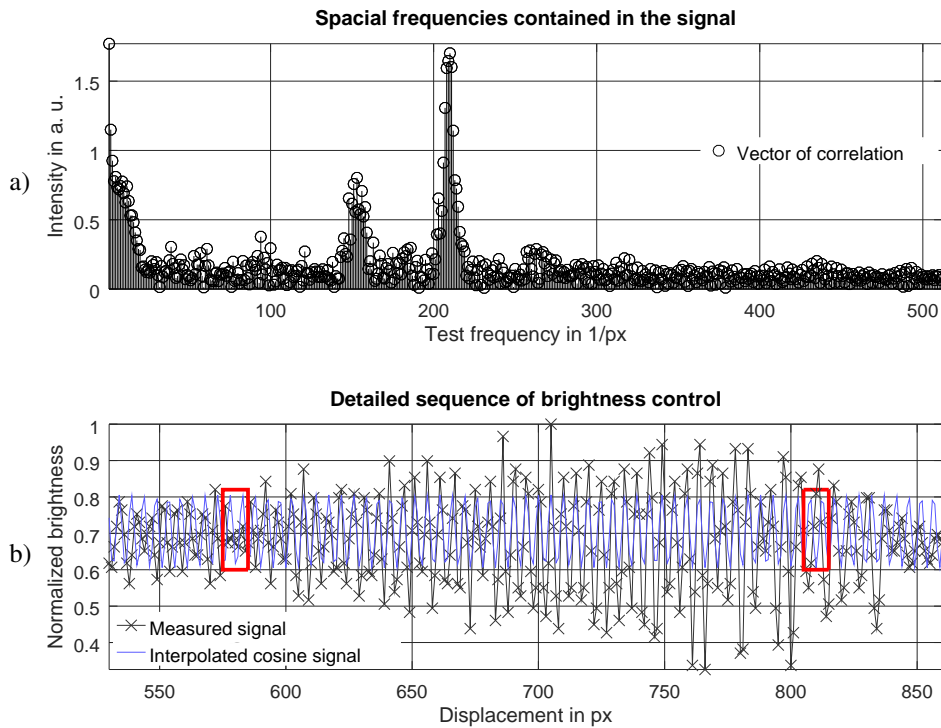


Fig. 6: Figure a) shows the spacial frequencies that are contained in the measured signal. The most present high frequency is 210 px. Figure b) presents a cut-out of the brightness control from the yellow framed section in Figure 5 superposed with a cosine function with frequency 210 px. The positions where the high frequency gets out of phase is marked with a red rectangle.

4. Validation setup for three dimensional particle tracking

The preliminary investigations give restricted insight to the capability of the imaging system and are therefore not eligible to infer if the system is suitable to undertake reliable research

on particle motion in three-dimensional complex plasmas. The expressiveness of theoretical parameters is limited by real world effects and assumptions that are made to create an effective algorithm for analysis. For example, thermal influence, lens quality, aging of the MLA, quality of the optical components as well as mapping of lenses and pixels. A reliable investigation on limits and capabilities of the optical system postulates an examination on particles in complex plasma. Since observation of static crystals is impossible due to the non-zero kinetic energy, a model system similar to the Ekoplasma setup needs to be established. The most similar system consists of a light source and a target likewise to complex plasma. The target has to meet the requirements mentioned below:

- Bulk material transparent in visible spectrum (VIS).
- All boundary surfaces of the bulk material are antireflection (AR) coated for VIS.
- Bulk material contains enclosed spheres with a diameter of about 100 nm up to 20 μm , that scatter or reflect incident light.
- Depending on the particle diameter, the spacing of the particles should be multiple times their radius.
- Target has to be specified; all parameters i. e. particle size, distance between particles, quality of the enclosed spheres should be well known.

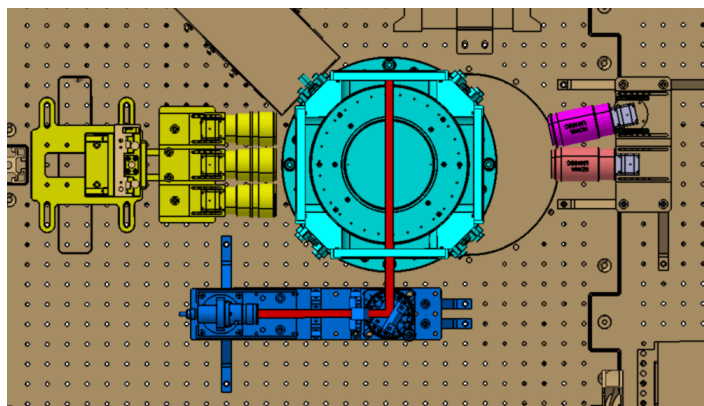


Fig. 7: The yellow components are the two dimensional cameras for general observation purposes. Blue is the laser diode with line optics; cyan is the plasma chamber, red the beam path of the laser, rose and purple cameras for the overview and observation of the plasma glow. The LF camera will be added in addition to this diagnostics.

In terms of illumination and scattering a two-dimensional target is inappropriate for the validation of the LF camera. A three-dimensional target is advantageous, though in the framework of this investigation several fabrication methods turned out to be unsuitable to fabricate a three-dimensional target. For instance, Two-Photon Polymerization is not applicable since the spheres are filled with undeveloped photoresist; by this they darken and the signal to noise ratio degrades with exposure to light and aging.³ Furthermore, the growth of a microstructure with Molecular Beam Epitaxy is limited to one direction and eliminates the growth of spherical defects.⁴ Embedding of nanoparticles on fused silica layers after etching holes inside is limited to pits

³Nanoscribe, 76344 Eggenstein-Leopoldshafen, Germany; e-mail 07-18-2017 from Jochen Zimmer.

⁴Physikalisch Technische Bundesanstalt, 38116 Braunschweig, Germany; e-mail 06-20-2017 from Frank Hohls.

of diameter $200\ \mu\text{m}$.⁵ Wet etching requires the spheres to be connected by capillaries, but they induce stray light in the model system.⁶ A hologram of a complex plasma sequence fails due to particle motion and the lack of an available adapted laser.

Finally, laser engraving turned out to be a promising fabrication method to obtain a three-dimensional target. For laser engraving a pulsed laser is focused inside a body from fused silica or acrylic glass. Not only the high energy density in focus leads to ionization and plasma formation inside the body which results in degradation of single dots. But also the high energy may lead to the emergence of microcracks due to thermal effects. Thus, the resulting structure is highly dependent on the properties of the engraving laser. That is why manufacturer Femtika⁷ provided a prototype for review purposes. Subsection 4.1 shows details of the review and subsection 4.2 gives detailed information of the final target design. In order to provide best illumination of this target the light source has to be tunable in terms of intensity and flexible in shape and focus. Two light sources are available. One is a dimmable but highly divergent white light that was equipped with appropriate optics during the experiments. The other is a dimmable laser (660 nm) with expanded beam shape identical to the line laser used in the Ekoplasma setup.

4.1. Review of the prototype

Figure 8 shows a sideways illuminated photomicrograph of the microstructure inside the prototype. The x-y plane is perpendicular to the engraving laser beam.

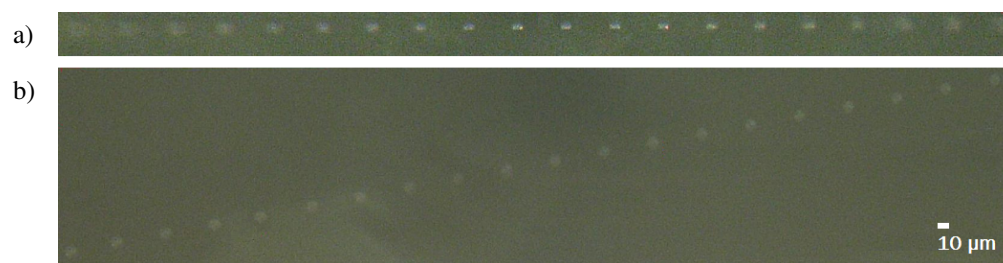


Fig. 8: Photomicrograph of the microstructure. The 20 defects are aligned inside bulk material from fused silica. a) shows the x-z plane and b) the x-y plane.

The microstructure consists from 20 three-dimensional defects with a diameter of about $(10 \pm 2)\ \mu\text{m}$. Figure 8 reveals slight elongation of the defects in z direction. Nevertheless, the defects are nearly spherical. The middle-to-middle spacing of two successive defects is about $(50 \pm 2)\ \mu\text{m}$. The extent of the structure in the x-z plane is about $(1000 \pm 10)\ \mu\text{m}$ and in the x-y plane about $(135 \pm 10)\ \mu\text{m}$ according to the measurement with the photomicrograph. Take notice, that the spacing of the defects is about 7 times closer than the particle spacing in an actual complex plasma crystal. First recordings sideways illuminated by laser light showed appearance of interference, thus only white light is investigated in the following.

Several photomicrographs sideways illuminated with white light are recorded for various angles of incidence. The incident light source is only moved in a circle around the prototype by that the reflected light remained perpendicular to the microscope for the entire measurement. Figure 9 illustrates micrographs illuminated under different angles of incidence. Further, the prototype is investigated with the LF camera. It is mounted on the optical bench in a way that the x-z direction points parallel towards the image sensor. The x-y plane is illuminated with white light. Figure 10 shows the experimental rig. Figure 11 contains the main information of this

⁵IPP toptec, 51101 Turnov, Czech Republic; e-mail 07-17-2017 from Vit Ledl.

⁶FEMTOprint, 6933 Muzzano, Switzerland, e-mail 07-25-2017 from Alexander Steimle.

⁷Femtika, www.femtika.lt up-to-date: July, 2017. 10224 Vilnius, Lithuania.

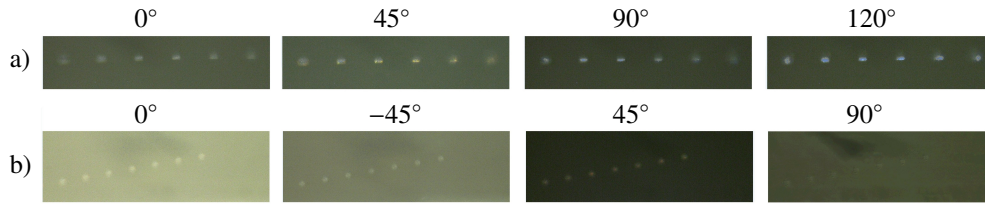


Fig. 9: Photomicrographs of x-z plane (see a) and x-y plane (see b)) sideways illuminated with different angles of incidence. The angles are mentioned above each image respectively.

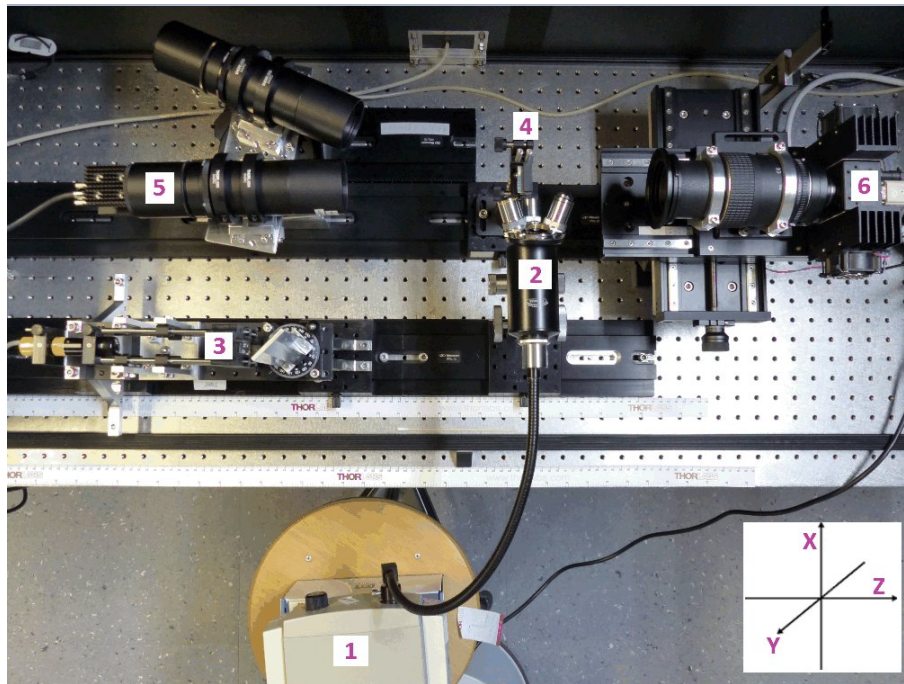


Fig. 10: Setup for Prototype review and model system. 1 denotes the white light source with 2 the collimating optics; 4 is the adjustable prototype mount and 6 tags the R5 LF camera. Devices 3 and 5 are extra. The directions are defined in the bottom right corner. The z axis also refers to the optical axis of the LF camera and the depth of field direction.

measurement. The microstructure is found to spread over 33 microlenses in the raw image. The reconstructed picture in total focus shows 20 tight spaced defects. The depth map that relies on the virtual depth of the image can be extracted from RxLive software and provides additional data. The depth map and its corresponding contour lines are presented. Metric measures are not attainable with RxLive. Figure 12 c) shows the turned target in the x-y plane. The quality of the reconstruction in the x-y plane is restricted due to stray light from the not refined outer surface of the prototype, see bright part of Figure 12 c). Despite the perturbation from stray light the 20 defects are visible and aligned in space. Contrary, the pattern from the reconstructed depth information in Figure 11 is not monotone aligned.

In order to study similarities and differences from defects to dust particles, the reconstructed images of the prototype in both planes are opposed to an image of complex plasma from a parabolic flight in 2015. The result is visualized in Figure 12.

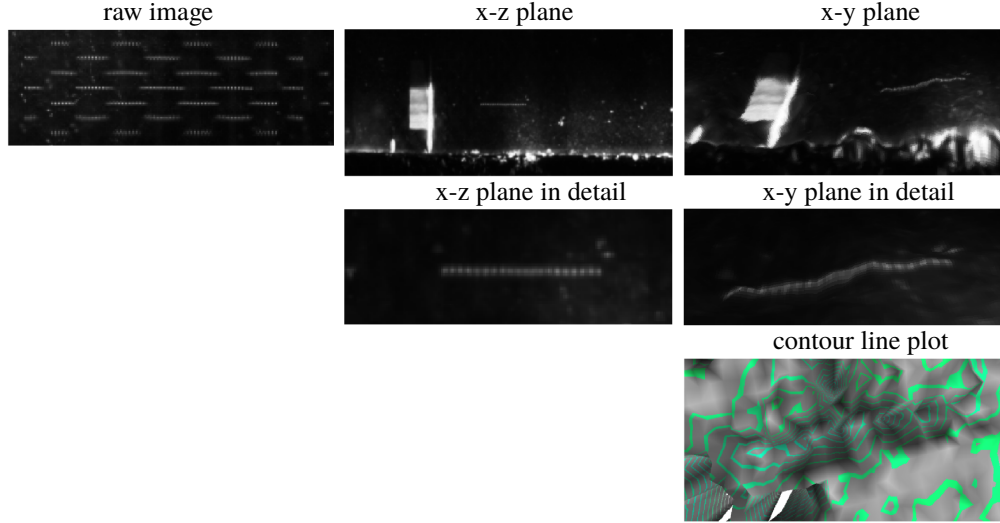


Fig. 11: The raw picture shows the image of the microstructure recorded on the CMOS sensor. x-z plane illustrates the reconstructed image in total focus; that is magnified in the detailed view. x-y plane is the depth image reconstructed from the depth measurement of the raw image; magnified in the detailed view. Contour line plot is a different graphic rendition of the depth image in bottom view. The curvature of the depth image is not monotone. The contour line plot gives about 6 spots with different depths levels.

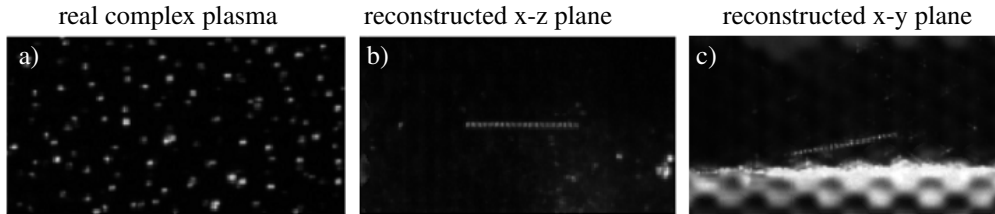


Fig. 12: Figure a) shows a sequence of real complex plasma from a parabolic flight in September 2015 taken with the present LF camera. b) and c) show the reconstructed image of the prototype in total focus in both planes respectively. c) shows 20 defects disturbed by stray light but with monotone inclination.

The brightness control of the x-y and x-z planes are collected and depicted in Figure 13. Several image sequences with about 50 frames are taken for the x-z plane while the entire setup remained fix. Later on, one sequence with 51 frames is used as input data for the RxFlow software to test the particle recognition and tracking algorithm implemented from Raytrix in the software RxFlow. Figure 14 shows a raw image of an arbitrary frame evaluated with RxFlow. The lens sets are distinct by the colors blue, green and red. Every bright spot encircled in green is recognized as a particle. Bright spots encircled in red are disregarded from further evaluation; this applies to spots that are detected in the boundary regions of lenses or that are inconsistent with the configuration parameters. Configuration parameters are for example minimal particle brightness, particle radius and background brightness. The output of RxFlow is a Cartesian coordinate (x , y , z) that comes along with a value for quality (Q). Every coordinate represents the center of a particle. The present License Dongle for the particle tracking software does not provide metric conversion. Hence a preliminary metric calibration is carried out with a pinhole that was illuminated with transmitted light and moved along a known trajectory. Further a bijective

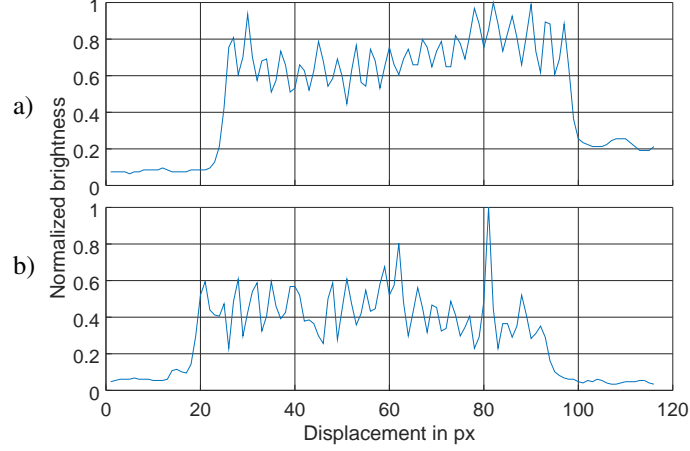


Fig. 13: Figure a) gives the brightness control of the prototype in x-z plane and figure b) in x-y plane. 20 peaks are visible in both planes. For a constant threshold not all peaks might be resolved or might be interpreted as an ensemble.

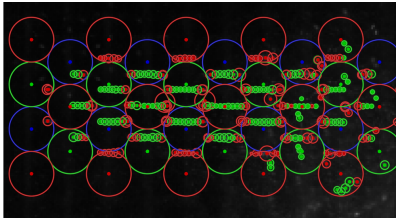


Fig. 14: Raw image of the particle recognition and tracking software RxFlow. Lens sets distinct by the colors blue, green and red. Bright spots encircled in green are recognized as particle while bright spots encircled in red are disregarded from further evaluation.

map was found to map the known trajectory onto the trajectory found by the tracking software. For rudimentary testing of the software capabilities the pinhole calibration is functional. For reliable data analysis this approach has to be repeated with a calibrated three-dimensional target. The quality of a detected particle is significantly affected by the number of matches in multiple lenses and the reprojection error. Figure 15 shows a superposition of the detected particles of 51 frames color-coded with their quality. Despite their quality the particles are found within a volume of $3.94 \times 4.51 \times 161.67 \text{ mm}^3$ in x-y-z direction. Particles with a quality greater than 0.7 spread less in space. Considering only the particles with a quality greater than 0.7 this volume reduces to $0.01 \times 1.18 \times 0.61 \text{ mm}^3$ in x-y-z direction. Compared with the outer dimensions of the microstructure this is a fair approximation. Table 1 lists the amount of particles identified in each frame with increasing overall quality.

Table 1: Average of detected particles in each frame with increasing overall quality

Q \geq	0	0.1	0.2	0.3	0.4	0.5	0.6	0.7	0.8	0.9	1
Average amount of detections per frame	32	23	21	17	15	10	8	5	3	3	1
Standard deviation	± 2	± 1	± 0								

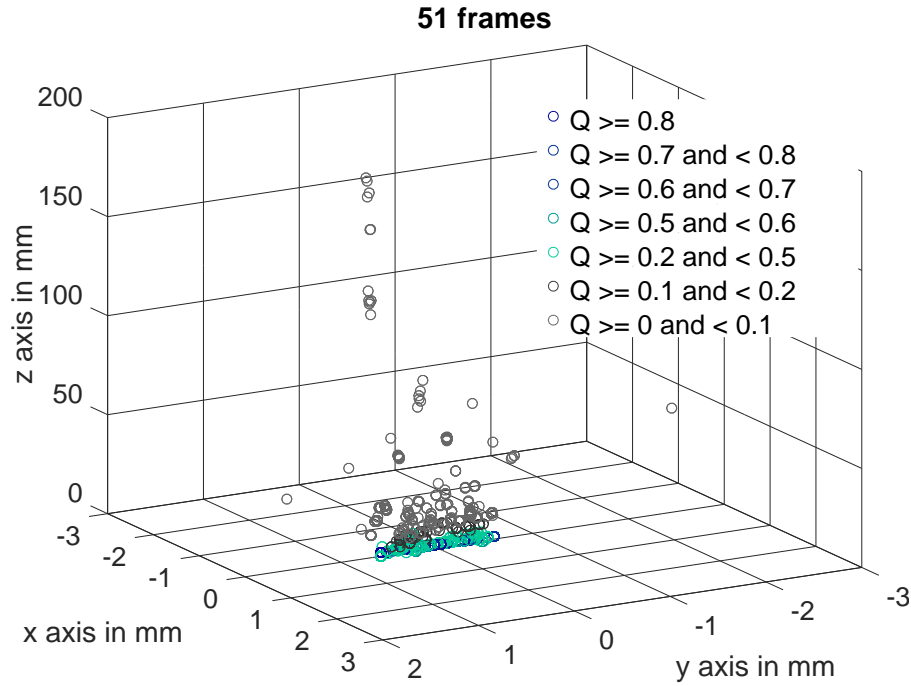


Fig. 15: Superposition of particle positions overall 51 frames linked to their quality Q . The prototype remained fix for the entire measurement. Unlike the 20 defects of the microstructure multiple particles were found.

RxFlow provides the assignment from particles in one frame to particles in the successive frames, aka tracks. Table 2 enumerates different locations of particles that are found in the whole sequence of 51 frames as well as tracks, taking the quality into account.

Table 2: Tracks of detected particles over all frames with increasing overall quality

$Q \geq$	0	0.1	0.2	0.3	0.4	0.5	0.6	0.7	0.8	0.9	1
Different positions overall 51 frames	289	201	178	142	130	94	70	51	22	17	5
Tracks in 51 frames	205	153	136	102	87	58	49	32	14	12	1

Figure 17 shows the tracks over the whole sequence for detected particles with a quality greater or equal than 0.9. Some tracks coincide in location, but exhibit a different track-ID. Several positions are found just once in the sequence; they are untraceable. Further, over all frames the detected defects and tracks with quality greater than 0.93 are the corner points. From this research several proposals can be derived for the validation target design.

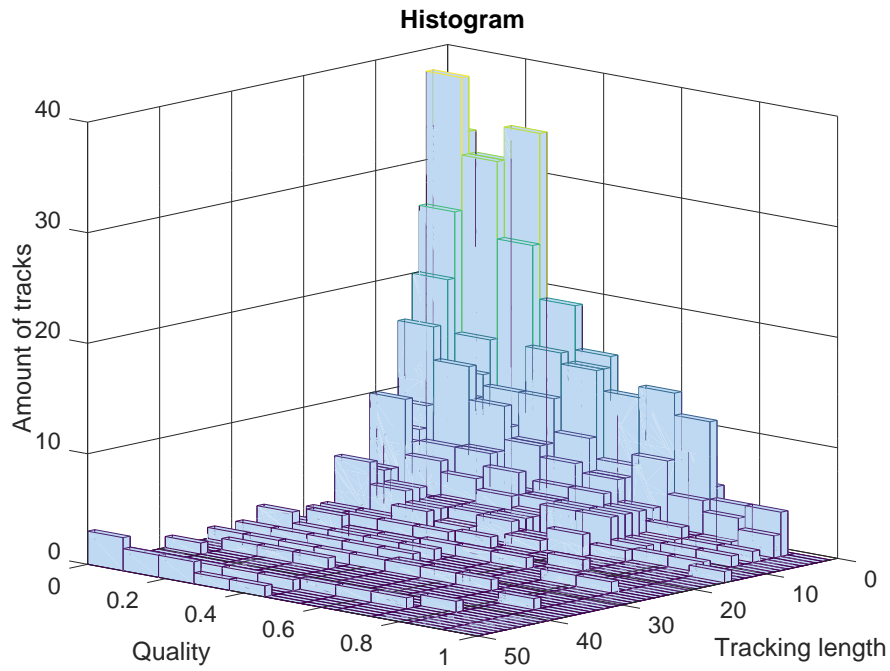


Fig. 16: The histogram links the tracking length with the quality and the amount of tracks over the whole sequence. It can be seen that the quality within one track varies and therefore the tracking length reduces as quality increases. For no quality factor the 20 defects can be recovered over the 51 frames.

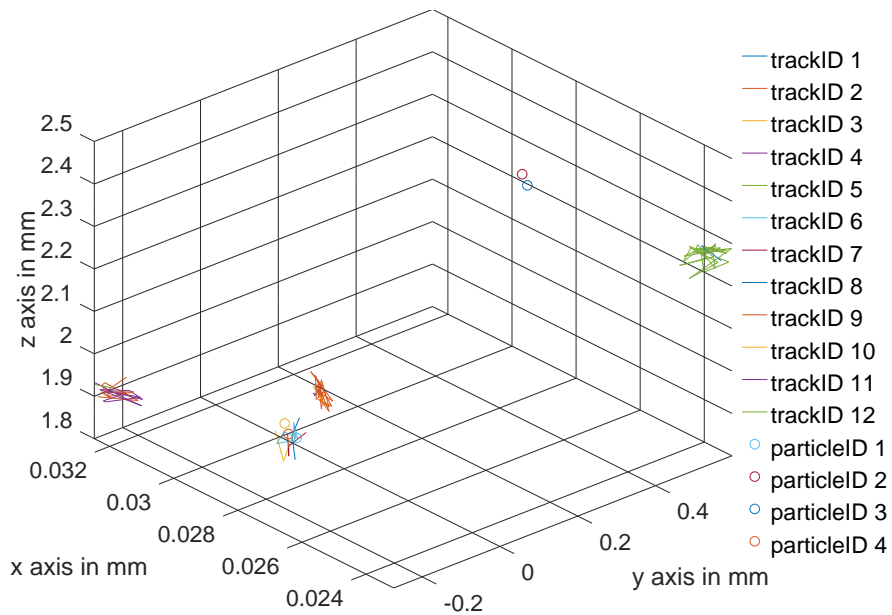


Fig. 17: For visualization connected tracks and single positions (particleID) with similar quality are illustrated. Several tracks superpose at the same position. Tracks are elongated in z-direction.

4.2. Target design

The architecture of the target is designed to undertake the most possible and meaningful investigations while keeping the microstructures away from each other to avoid mutual interference. Over all, three self contained patterns are designed. They are distributed into two separate cuboids from fused silica each less than 3 mm thick to warrant least defect elongation. The first and the second pattern are in the same bulk material. The third pattern is embedded in a separate cuboid. Figure 18 illustrates the patterns.

The first pattern aims to investigate the resolving power of the RxFlow software in terms of particle density. 17 defect tuples with different distances are planned to be engraved into the cuboid. They have a diameter of 10 μm this corresponds to the average particle size used in Ekoplasma. In the future each pair will be illuminated separately with white light, recorded with the RxLive software and analyzed with RxFlow software. This pattern can be used for metric calibration. Movement along a known trajectory simulates particle motion and allows for the conversion of Rx units into real world metric measures.

The second pattern intends to examine the influence of the particle diameter on the particle tracking analysis. It consists from 8 defect tuples with different distances, while every tuple has a particular diameter. Likewise to the first pattern each pair is illuminated separately, recorded with the RxLive software and analyzed by the RxFlow software.

The third pattern simulates a three dimensional complex plasma crystal in hexagonal closed package arrangement. The defects fill an over all volume of about $6 \times 2 \times 2 \text{ mm}^3$, with defect diameter of 10 μm and lattice constant of 0.35mm. The lattice constant corresponds to the outcome of previous research on complex plasma crystals. It aims to test the quality of the multi particle tracking isochronal in all three dimensions and will further reveal problems like artificial pairing of particles. In addition the third pattern facilitates the testing and development of a three dimensional light source for the Ekoplasma chamber. Since the current line laser is not capable of three dimensional illumination it requires modified optics or replacement by an intense light source that has to be validated.

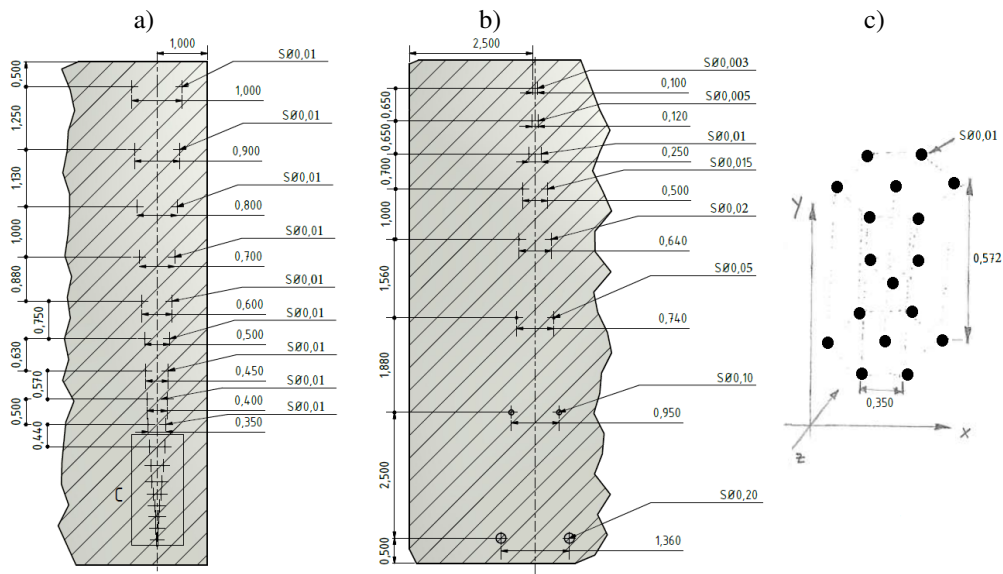


Fig. 18: Detailed image sections of a) first, b) second and c) third pattern. a) and b) are embedded in the same bulk material. Hexagonal lattice is engraved in a separate cuboid.

5. Results and Discussion

Raytrix claims a lateral resolution of 1 megapixel instead of the 4 megapixel from the actual Baumer CMOS chip, considering the camera design this seems reasonable. A traditional stereoscopic setup consisting of two or more cameras, with an equivalent CMOS chip has therefore a better lateral resolution but without the possibility of refocusing. Best working distance is about (123 ± 0.2) mm in front of the camera, which is suitable for the application in the Ekoplasma setup. The spacial resolution of the R5 is not homogeneous over the field of view. **Boundary effects?** Especially for delicate patterns towards the depth of field direction this volume reduces. The depth of focus in the center of the field of view for $15 \frac{\mu\text{m}}{\text{mm}}$ is limited to a range of (3.196 ± 0.2) mm. The continuous decay over principal distance for the lateral field of view needs to be investigated with an adapted target, that was not present during this internship. However, comparison of the lateral brightness control graphs show that element 4 of group 4 can be marginally resolved while element 5 of group 4 is non-resolvable. This corresponds to $25.39 \frac{\mu\text{m}}{\text{mm}}$ but only for a tight area in the center of the camera.

Evaluation of the microstructured prototype showed that laser engraving is suitable to manufacture a device that is capable to simulate particles in complex plasmas. Artificial defects resemble real particles in shape and size. Additional investigations unveiled that the defects are not perfectly spherical. Illumination by the laser showed the appearance of interference. As demonstrated this is not the case for white light illumination. The spherical defects remain in place and maintain their spacial extend in good approximation for different angles of incidence. In the future the relative position of the light source and the target will stay fixed, they will be moved as a unit. Illuminated with white light the defects show slight dispersive characteristics this may lead to disadvantages and should be kept in mind. However, white light reflection is demonstrated to be the dominant process over the entire defect area. The brightness control of the prototype (see Figure 13) and Table 1 illustrate that the present prototype is neither suitable to undertake a verification of the RxLive and RxFlow software nor a metric calibration. Due to the fact, that the defect density greatly exceeds the particle density of a complex plasma. However, the least perturbed defects on the edges of the microstructure are recognized as single particles with a high quality this implies that a laser engraved defect is suitable to simulate a complex plasma.

Figure 11 a) and b) show that the reconstruction is somewhat broadened compared to the raw picture. Slight movements along the optical axis resulted in only sixteen peaks, this implies artificial sampling of close particles which are not related to each other in the first place. Manufacturer Raytrix pointed out without further quantization that high particle densities can not be resolved. Hence, the significance of this measurement is limited to the conclusion that the microstructure is observable with the LF camera for a particular focal distance. Besides, the reconstructed depth map shows large derivation from linear behavior. Considerably, the depth map shows unexpected curvature whose contour line is not consistent with the present microstructure. In addition, the quality of the x-y plane microstructure implies that it is important to govern a certain distance between the microstructure and the outer surface of the bulk material. Further, it is applicable to refine the boundary surfaces. To a greater extent, light from defects are superposed with light from another origin, this results in a deformation of the spots and can lead to create artificial pairing. Prospective examinations have to test in detail if three dimensional structures show artificial pairing as for high particle densities or stray light. This investigations are feasible with the target designed in the framework of this internship. Concluding, due to its design the target provides the same capabilities for every imaging system. It therefore is a universal device that will help to develop and classify an imaging system applicable for three dimensional plasma research.

6. Conclusion

In the framework of this project the main features of a light field camera were explored. A three-dimensional calibration target for the validation process of light field cameras in the field of complex plasma research was designed. The identification of a suitable fabrication method was a major topic. Engraving of microstructures in a bulk material from fused silica turned out to create a device that is eligible to simulate particles in complex plasma. Future investigations should test whether the three-dimensional structures can be fully recovered with the light field camera or if artificial pairing occurs as for high particle densities or stray light. Furthermore, the closest resolvable particle spacing has to be found. Each of this investigations can be carried out with the commissioned target. The findings open up a series of new experimental setups to investigate the feasibility of light field cameras in complex plasma research and compare them with the eligibility of traditional stereoscopy.

Glossar

Abbreviation	Description
AR coating	Antireflection coating
CMOS	Complementary metal-oxide-semiconductor
DLR	Deutsches Zentrum für Luft- und Raumfahrt / German Aerospace Center
DOF	Depth of field
ISS	International Space Station
MLA	Multi lens array
LF	Light field
R5	Serial number of the present light field camera
RxFlow	Commercial particle recognition and tracking software
RxLive	Commercial image reconstruction software for light field cameras
Imaging system	Combination of optical device to capture light and data processing unit
Track-ID	Identification number for a particular track
USAF	United States Air Force
VIS	Light in the visible spectrum (400nm-800nm)
Q	Quality factor